Accepted manuscript for *Desalination*

Volume 540, 15 October 2022, 115980

https://doi.org/10.1016/j.desal.2022.115980

Arch-type Feed Spacer with Wide Passage Node Design for Spiral-Wound Membrane Filtration with Reduced Energy Cost

Jia Yu[a1], Dengyue Chen[b1], Jun Jie Wu[c], Bing Wang[a*], Robert Field[d,e]

[a] *College of Environmental Science and Engineering/Sino-Canada Joint R&D Centre for Water and Environmental Safety, Nankai University, Tianjin 300071, PR China*

[b] *School of Pharmaceutical Sciences, Xiamen University, Xiamen 361005, Fujian, PR China*

[c] *Department of Engineering, Faculty of Science, Durham University, Durham DH1 3LE, UK*

[d] *Faculty of Engineering and Environment, Northumbria University, Newcastle NE1 8ST, UK*

[e] *Department of Engineering Science, University of Oxford, Oxford OX1 3PJ, UK*

[#] J Yu and D Chen contributed equally to this work and should be considered as co-first authors.

* Corresponding author: B Wang, bwang@nankai.edu.cn

Abstract

A novel feed spacer for spiral-wound membrane modules is proposed. Based upon a continuous arch-type streamline frame two feed spacers with different node designs were constructed. In the first, Arch-Hole, two elliptic cylinders form a node zone with a passage. The other, named Arch, has a solid node. Their hydrodynamics, fouling and filtration performance were compared with a commercial design. This was a classic net-type spacer with nodes of relatively substantial size. All three were manufactured using 3D printing. Computational fluid dynamics simulation showed that the Arch-Hole design gives a more uniform velocity distribution with fewer dead zones. Subsequent evaluation of this design indicated less foulant accumulation as confirmed by optical coherence tomography and the evolution of channel pressure drop. Measured adenosine triphosphate and total organic carbon values for the module with this spacer were substantially lower than the corresponding values associated with the commercial design. Crucially with the Arch-Hole design, flux values remained higher than for the other two designs. Thus use of this spacer would minimize both capital and operational costs. Compared to the commercial one, use of the Arch-Hole design would reduce the energy cost of filtration significantly beyond the 69% found for the application considered herein.

Key Words

Feed spacer; Computational fluid dynamics; Spiral-Wound Membrane; Fouling; Specific energy cost.

Nomenclature

ATP	Adenosine triphosphate
C_b	Bulk solute concentration
CFD	Computational fluid dynamics
CP	Concentration polarization
DI water	Deionized water
FCP	Feed channel pressure drop
k	Boundary layer mass transfer coefficient
OCT	Optical coherence tomography
SWM	Spiral-wound membrane
SEC	Specific Energy Consumption
TDS	Total dissolved solids
TOC	Total organic carbon
U_F	Feed flow velocity

1. Introduction

Spiral-wound membrane modules (SWM) has been widely used in water filtration due to their small footprint and high specific surface area [1, 2]. Such modules are at the heart of seawater desalination technology. The feed spacer inside the module is an indispensable component to not only support the membrane but promote turbulent flow and reduce concentration polarization [3]. However with the evolution of fouling (and some fouling is inevitable) there is a propensity for feed spacers to create some dead zones and further promote fouling including biofouling. Thus, the existing design of feed spacer can typically result in higher pressure loss across the module [4, 5]. There is a consequential lowering of permeation flux [6-9] and together with the increased trans-module pressure drop, a resulting increase in the specific energy cost. Whilst, the biofouling on the membrane surface is flux-driven, with a lesser dependence on cross-flow; biofouling on spacers can be observed by the rise in feed channel pressure drop (FCP). Membrane biofouling is mainly flux driven and can be observed by flux decline, or for operation at a constant flux, by a rise in TMP. In contrast spacer biofouling generates the aforementioned augmentation of FCP [10, 11]. As a result, feed spacer design has attracted attention with the aims of enhancing process efficiency and thereby reducing the relative energy consumption [12].

Prior studies have shown that feed spacer geometry can have a significant influence on the hydrodynamics inside the flow channel [13]. Generally, researchers have mainly focused on the influence of geometric parameters of the traditional net-type feed spacer on hydraulic performance and have studied the flow attack angle (α), mesh angle (β), filament spacing/mesh size (l) and filament diameter (d) [3, 14-16]. Moreover, the hydrodynamics changes induced

by geometric variables have a significant effect on the filtration performance [17-21].

To understand the closest analysis between feed spacer design and its effect on filtration characteristics, computational fluid dynamics (CFD) is a powerful tool to obtain the hydrodynamic behavior [17, 22-24]. The flow velocity field, shear stress, mass transfer and feed channel pressure drop (FCP) can be predicted through CFD simulation [25-28]. Combining the CFD and experimental results, a commonly agreed view is that shrinking the filament spacing reduces FCP [29, 30].

The spacer node is another important parameter, since the flow velocity reduces after the flow has passed and the low velocity zone can become a dead zone that initializes biofouling. The spreading of biofouling results in higher FCP and higher specific energy consumption [31-36]. It has been found out that an open-pore structure in the spacer node (which permits fluid to flow through the node hole) is superior because increases the flow velocity after the node and thereby reduces dead zones [36, 37]. In turn this affects membrane fouling and thus permeation flux.

The complicate relation between the hydrodynamics effect and the fouling performance has recently received more attention, and the findings suggest that velocity non-uniformity and dead zones inside feed channel are the main reasons for foulant accumulation [38-41]. Ali et al. [35] proposed a new turbine feed spacer, in which the blades rotated at a high speed under the impact of water flow to form a strong fluid jet, thereby generated turbulence in the feed channel. It found that the flow velocity and shear stress were evenly distributed, which effectively limited the accumulation of foulants and further reduced FCP. In addition, the thickness of filament could be manufactured to be smaller, in other words, the gap zone

between filament and membrane became larger, by which the flow velocity through this gap could be effectively decreased, and the velocity uniformity was enhanced. This design improved the fouling control and filtration performance as well as the energy consumption [34].

The development of 3D printing technology enables fine-size, complex structures suitable for feed spacers to be produced in a fast and economic way. Hence, 3D printing technology should promote the development of novel feed spacer for experimental investigations into the effects of spacer geometry. Although the number of investigations is growing, progress is still in general quite limited [34, 35, 42-44]. Therefore, the overall objective of this work is to quantify the hydraulic and fouling performance of a novel feed spacer design, under different operating conditions. This was accomplished by a study encompassing 3D printing technology for manufacture, conducting CFD simulations and fouling experiments to obtained detailed information on the performance of feed spacer. Two arch-type feed spacers were designed. The Arch-Hole geometry combined the advantages of a drop-like frame and node-opening, the other design without the node opening was named Arch. The hydraulic performance was studied in detail at various cross-flow velocities of 0.03 ~ 0.27 m/s, with special attention paid to the determination of velocity profile and shear stress distribution. The anti-fouling characteristics were studied by a 5-day fouling experiments, with OTC scan images and measurements of TOC, ATP, FCP and specific flux in the channel. Those data were also compared with a standard commercial feed spacer.

The use of constant pressure ensures that all feed spacers were evaluated for the same transmembrane filtration pressure, which permitted evaluation as to whether the permeate flux changed with spacer design. Whilst our study was focused on exploring the effect of changes

in overall performance due to changes in the spacer geometry under constant pressure conditions, further work at constant flux would be valuable.

2. Methods and materials

2.1 Feed spacer designs

The two Arch-type feed spacers and the commercial feed spacer had the same node height of 1.2 mm. The arch-type feed spacers had non-varying diameter of 0.5 mm, which included two structures i.e., Arch and Arch-Hole. Both of them had the same node shape of ellipse cylinder. The difference is that the node of feed spacer Arch is a solid elliptical cylinder, whilst Arch-Hole is composed of two small elliptical cylinders with height of 0.35 mm, which creates a relatively wide passage for flow at the node. The detail structure and dimensions were shown in Fig. 1 and Fig. S1.

The feed spacers designed in this work were manufactured by 3D printer (3Dsystems, Mjp3510HD, USA), with printing accuracy of 0.025 mm and resolution of 16-33 μm, which can accurately print and restore the target feed spacers. The material used in printing is VisiJet Crystal (photosensitive resin) with high durability and stability. The feed spacers were all printed to the required size and used in the subsequent filter modules.

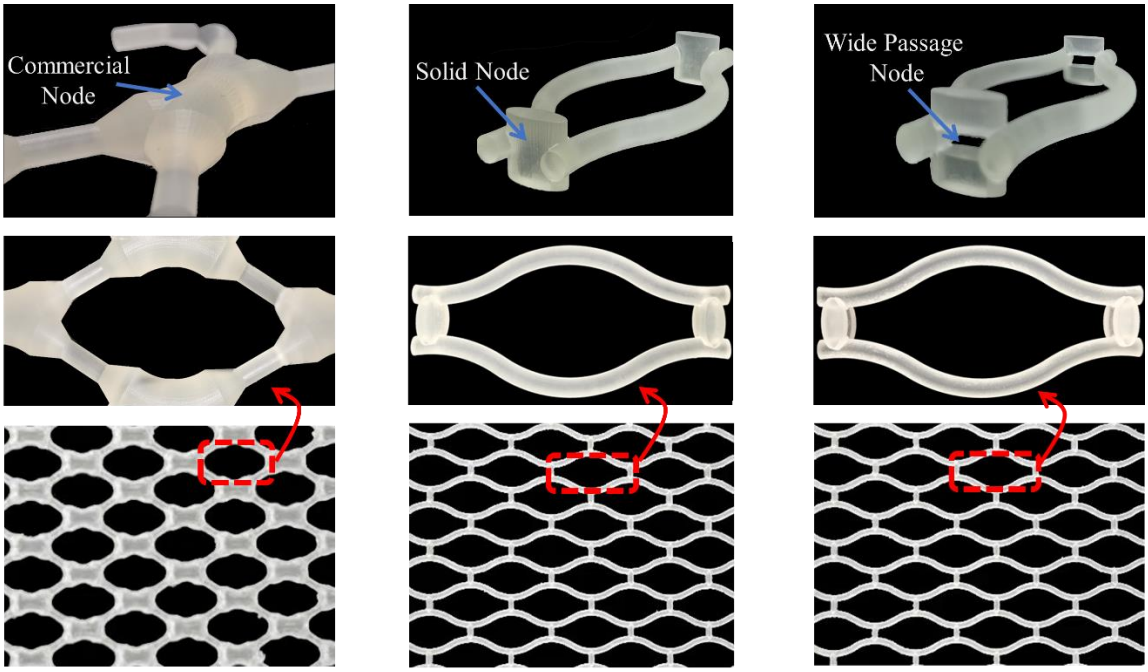

Fig. 1 Schematic diagram and the prototype of standard and arch-type spacers at various orientations.

2.2 Experimental set-up

Experiments were conducted in a filtration system, which included three parallel membrane modules each with one of the three different feed spacer designs. NF membrane (NF2, Zhongke Ruiyang, China) was used for nanofiltration process, which has a $MgSO_4$ rejection of 99% (with 2000 ppm and 0.48 MPa). The schematic diagram of the filtration system is shown in Fig. 2. Feed water was send from the 50 L feed tank to the crossflow cells (66 × 40 × 1.2 mm) by the booster pump (CHLP-RP, NURET, Italy) which maintained the working pressure. Instrumentation included flowmeters and differential pressure transmitters (EJX110A, YOKOGAWA Electric Corporation, Japan) to monitor the feed channel pressure drop (FCP) Permeate water was collected and weighed by a digital balance. A transparent

window in the crossflow cells enabled observations by an optical coherence tomography (OCT) (OPIMG, Optoprobe, UK) of the growth of the fouling layers. The feed tank was kept topped up by adding water and nutrients on daily or twice daily basis.

-

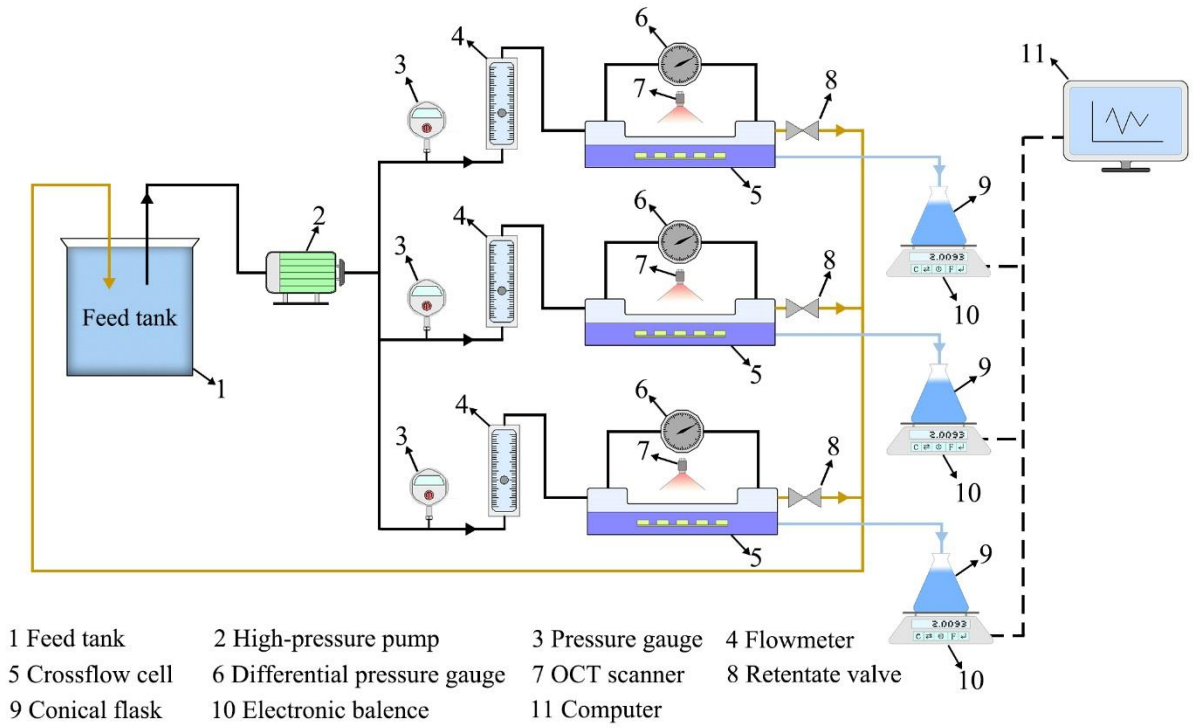

Fig. 2. Schematic diagram of a laboratory-scale filtration set-up.

2.3 Operating conditions

Before the fouling test, the membranes were rinsed in deionized (DI) water for one day. Then, membrane was soaked and compacted by DI water with 0.48 MPa (optimal working pressure of NF membrane) for at least 12 hours (hrs) until the permeation became stable. The results showed that the initial flux of Arch-Hole, Arch and Commercial systems were 28.8 LMH, 23.9 LMH and 22.7 LMH, respectively. These values are comparable to those used elsewhere e.g. [11]. Afterwards, ultrapure water was used to conduct a hydraulic test to

evaluate the hydrodynamic performance of different feed spacers. After the hydraulic test was completed, the feed water was replaced with synthetic feed solution to conduct fouling test.

The synthetic feed solution was prepared to provide nutrients required for biofilm formation, which can stimulate fouling faster in 5-day experiment. The biomass developed as a result of opportunistic bacteria in the feed water. The feed solution was prepared by adding various nutrient to tap water, namely sodium acetate, sodium nitrate, monosodium phosphate, magnesium chloride and calcium chloride. The dosage was 0.5 mg/L Mg^{2+}, 0.5 mg/L Ca^{2+}, 2 mg/L C and C: N: P mass ratio of 100:20:10. The solution pH value was adjusted to be 10 by sodium hydroxide, in order to prevent bacterial growth in the dose container [40].

2.4 Biomass analysis

After conclusion of the fouling experiment, the membrane and feed spacer were removed for ex-situ analysis. Samples were prepared to ascertain TOC (used to reflect the content of organic carbon) and ATP (used to indicate microbial activity). These measurements enable one to characterize the accumulation of foulant.

Organic contamination on the surface of membrane/feed spacer [45] was assess by firstly cutting samples of size 1×2 cm from the membrane and feed spacer. Then secondly the samples were placed in a centrifuge tube, and put in a 0.2% HCl solution (pH=1.3), soaked in a shaker at 150 rpm with constant temperature of 25°C for 24 hrs. Thirdly, 10 mL of 0.26% NaOH solution was added to the previous centrifuge tube and soaked for 24 hrs. under the same condition as above. After the immersion had been completed, the solution was passed through a 0.22 μm membrane filter which was then inserted into a total organic carbon analyzer (multi N/C3100, Jena, Germany) for TOC measurement. TOC levels were expressed as the total

organic carbon per square centimeter. The membrane area when evaluating membrane is themselves, for the spacers, it referred to the membrane surface that the spacer occupied.

The accumulated biomass and activity on the membrane / feed spacer can be characterized by the content of ATP [12]. Again 1×2 cm samples of membrane / feed spacer were taken. They were put into a centrifuge tube containing 1.5 mL sterile physiological saline, then mixed and shaken for 3 minutes to extract the biomass into the solution. The above extraction process was repeated three times. In accord with the luciferase method, the Bactite Glo ™ microbial cell viability assay kit [46] was used to determine the ATP content in the extract.

2.5 CFD simulation

The geometry of computational domain of the feed spacers were established by GAMBIT 2.4.6 software. Subsequently, numerical simulation was carried out in ANSYS Fluent 14 to study the hydrodynamics of different feed spacer geometry and compared with experiment results. Fluid flow phenomena, assuming incompressible Newtonian fluid, without energy exchange, involved two conservation laws: conservation of mass and conservation of momentum. The flow was proposed as a steady-state laminar flow, and the fluid medium is taken to be pure water (temperature 25 ℃, density 997 kg/m^3, dynamic viscosity 8.899×10^{-4} Pa·s). Hence the following continuity (Eqn. 1) and momentum (Eqn. 2-4) equations were considered. Modelling outputs (as shown below) compared well with the experiment output and this provided good justification for the CFD assumptions.

$$\frac{\partial \mathrm{u}}{\partial \mathrm{x}} + \frac{\partial \mathrm{v}}{\partial \mathrm{y}} + \frac{\partial \mathrm{w}}{\partial \mathrm{z}} = 0 \quad (1)$$

$$\mathrm{u}\frac{\partial \mathrm{u}}{\partial \mathrm{x}} + \mathrm{v}\frac{\partial \mathrm{u}}{\partial \mathrm{y}} + \mathrm{w}\frac{\partial \mathrm{u}}{\partial \mathrm{z}} = -\frac{1}{\rho}\frac{\partial \mathrm{P}}{\partial \mathrm{x}} + \frac{\mu}{\rho}\left[\frac{\partial^2 \mathrm{u}}{\partial x^2} + \frac{\partial^2 \mathrm{u}}{\partial y^2} + \frac{\partial^2 \mathrm{u}}{\partial z^2}\right] \quad (2)$$

$$u\frac{\partial v}{\partial x}+v\frac{\partial v}{\partial y}+w\frac{\partial v}{\partial z}=-\frac{1}{\rho}\frac{\partial P}{\partial y}+\frac{\mu}{\rho}\left[\frac{\partial^2 v}{\partial x^2}+\frac{\partial^2 v}{\partial y^2}+\frac{\partial^2 v}{\partial z^2}\right] \quad (3)$$

$$u\frac{\partial w}{\partial x}+v\frac{\partial w}{\partial y}+w\frac{\partial w}{\partial z}=-\frac{1}{\rho}\frac{\partial P}{\partial z}+\frac{\mu}{\rho}\left[\frac{\partial^2 w}{\partial x^2}+\frac{\partial^2 w}{\partial y^2}+\frac{\partial^2 w}{\partial z^2}\right] \quad (4)$$

where u, v, w represents the velocity components in x, y, z coordinate system (m/s), ρ is the liquid density (kg/m^3), μ is the dynamic viscosity, P is the pressure (Pa).

The total number of grids in the computational domain is approximately 880,000. Mesh independent verification was carried out to confirm that there is no change of calculation results by increasing the number of grids. The inlet flow rate is in the range of 0 ~ 0.18 m/s. Considering that the permeation velocity of the membrane is much lower than the cross-flow velocity, the bottom of the channel was assumed to be an impermeable surface, and no-slip wall conditions were applied on the channel wall and the surface of feed spacer.

3. Results and Discussion

3.1 Hydraulic characterization of feed spacers

CFD simulations were performed on the three test feed spacers at the cross-flow velocity corresponding to the experimental conditions. The hydraulic characteristics induced by different feed spacers is mainly described in this section. On one hand, these results validate the CFD model, and on the other hand, they show which geometry is more advantageous in improving pressure drop performance.

Fig. 3 (A) presents the FCP drop induced by different shapes of feed spacer as a function of crossflow velocities. As the velocity increases, the FCP drop increased in all cases. Both Arch and Arch-Hole feed spacers generated lower pressure drops than that from the commercial one, indicating that the drop-like shape is more advantageous than the traditional

straight-lined commercial shape. The Arch-Hole feed spacer always had the smallest pressure drop performance.

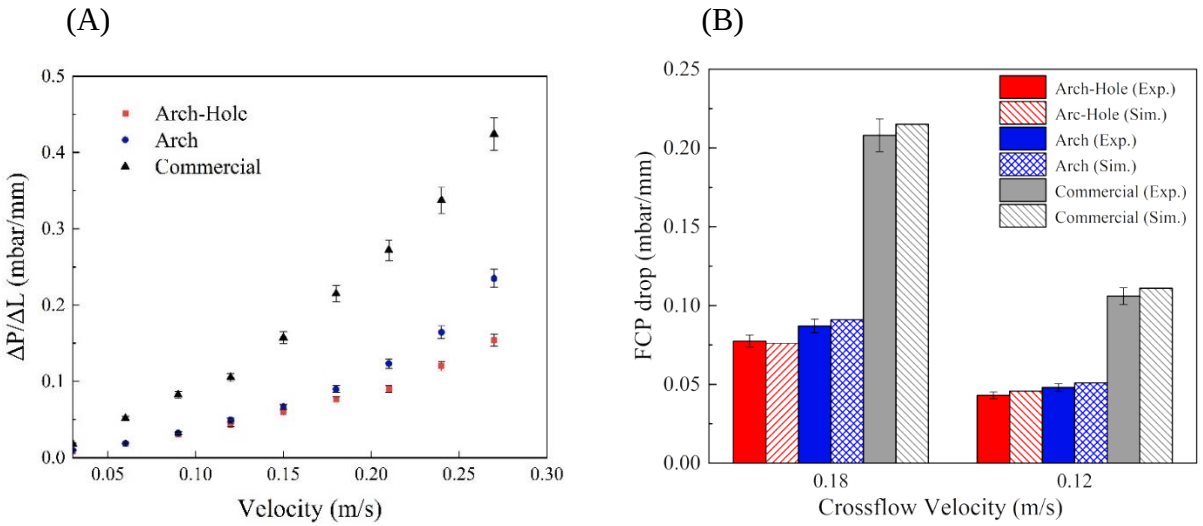

Fig. 3 (A) Comparison of experimentally measurements of feed channel pressure (FCP) drop with crossflow velocity for the three different spacer-filled channels, (B) Comparison of simulation results at two different crossflow velocities (0.12 m/s and 0.18 m/s) with corresponding experimental results.

As shown in Fig. 3 (A), there is no obvious difference between the Arch and Arch-Hole designs at cross flow velocities up to 0.12 m/s, the pressure drops of Arch-Hole and Arch were 0.043 and 0.050 mbar/mm respectively. However, as the velocity became larger, the difference between the two structures became significantly, especially after the velocity of 0.24 m/s, FCP from Arch feed spacer increased steeply. The difference between two structures reached to be around 0.12 mbar/mm. This indicated that small variation of node in Arch-Hole design could result in the advantage of lower FCP at larger crossflow velocities.

Additionally, the FCP results from simulation and experiments were compared in Fig. 3 (B). The error was less than 5%, indicating good agreement between CFD and experiment results thus this robust CFD model could be used in future to explore other related designs. At a feed velocity of 0.18 m/s, the difference between two drop-like feed spacers was larger than that of small speed of 0.12 m/s, which was also observed in Fig. 3 (A). This could be somehow explained by the velocity distribution from CFD. In the simulation results, as shown in Fig. 4, the velocity distribution in the center plane of channel at a velocity of 0.12 m/s has been compared for three structures of feed spacer.

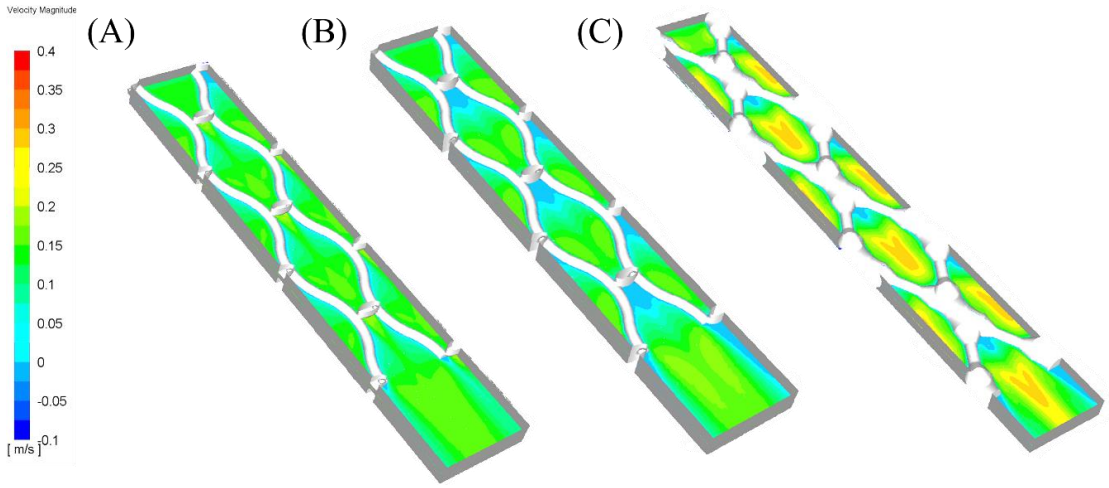

Fig. 4 Comparison of numerically simulated x-velocity contours at the central plane of the channel for (A) Arch-Hole, (B) Arch and (C) Commercial spacers at U_F = 0.12m/s.

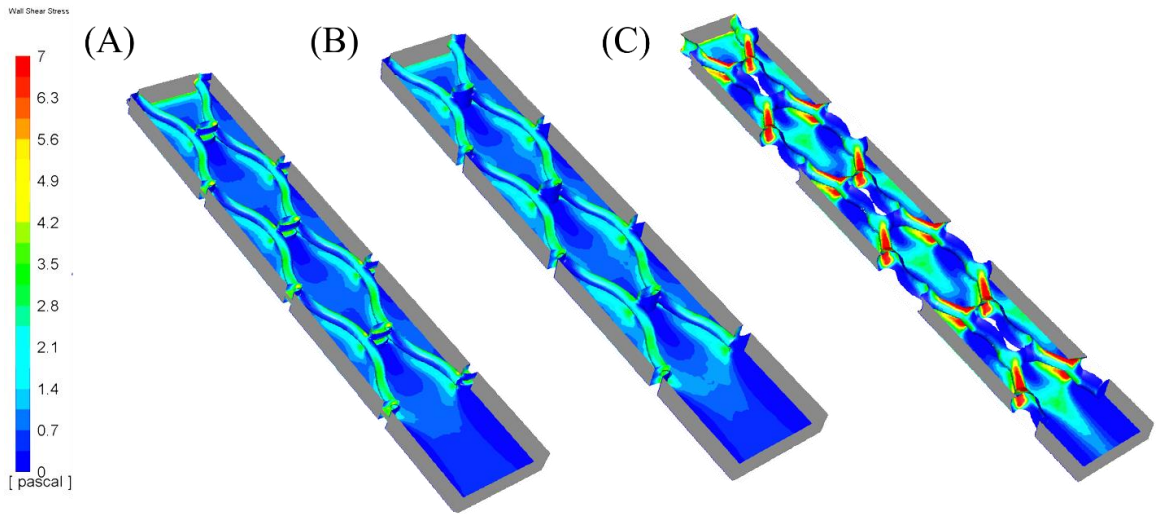

Fig.5 Comparison of numerically simulated shear stress contours for (A) Arch-Hole, (B) Arch and (C) Commercial spacers at U_F = 0.12m/s.

Along the fluid flowing direction, before and after the commercial node there were large dead zones with the commercial spacer. For Arch and Arch-Hole designs, one can view the structure as essentially consisting of two elements, streamlined filaments or curved struts that and a series of nodes with four filaments being joined at each node. This design has reduced the area of dead zones, and the hydraulic angle formed by the streamlined nodes allowed fluid to flow smoothly around the feed spacer nodes, especially with the Arch-Hole design which generates a micro jet at the nodes. This produces a higher velocity after the nodes compared with the other two feed spacers and thereby eliminates the "dead zones" at the nodes. According to the CFD simulation results (Fig.5), it can be seen that the shear stress of the Arch-hole is the most uniform, and the shear force at the node is greater than that of the Arch.

3.2 Fouling accumulation

Images of feed spacer and membrane were taken after fouling experiments and are shown in Fig.6. From a macro point of view, it can be clearly seen that the greatest amount of

accumulated foulant is on the commercial spacer with there being significant accumulation at the nodes. There are fewer foulants in the case of Arch and the least for the Arch-Hole design. The same trend was observed for the membrane surface, with fouling in the commercial case being the most serious and Arch-Hole case yielding the least.

This indicated that the Arch-Hole design can effectively reduce the fluid dead zones especially at the node area. In addition, combined with the velocity distribution of CFD simulation (Fig. 4), it can be deduced that velocity distribution of Arch-Hole has the greatest uniformity and that the reduction in dead zones will result in less foulant accumulation.

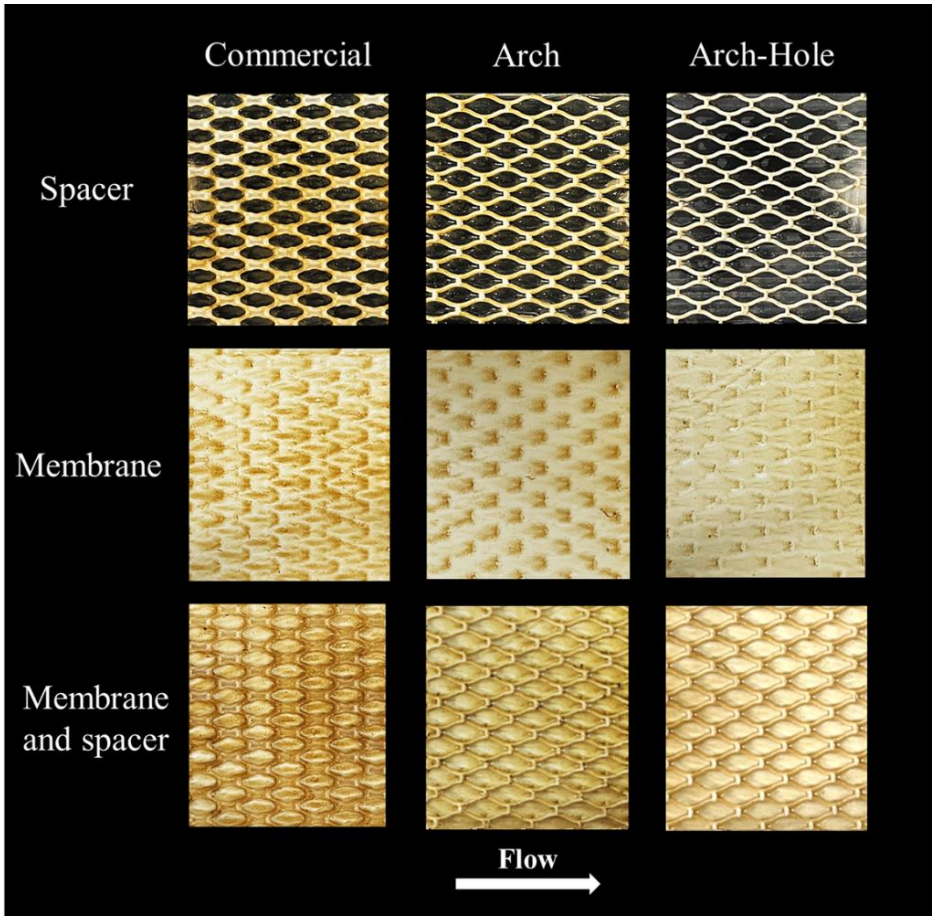

Fig. 6 Mapping the biofilm attachment/growth with hydrodynamics conditions at constant inlet feed velocity for various spacers.

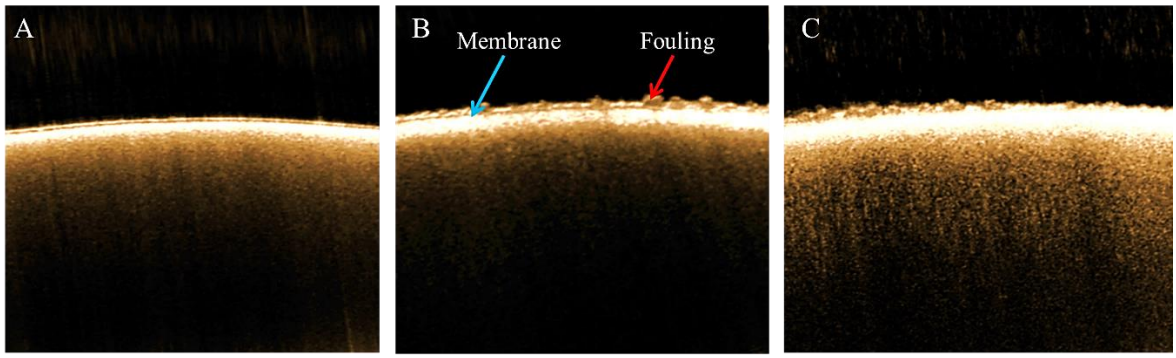

Fig. 7 OCT scans for fouling taken on the membrane surface after 5 days, Arch-Hole (A), Arch (B) and Commercial (C).

Biofouling accumulation on the membrane surface was analyzed and compared through OCT scans. The results which are illustrated in Fig. 7 showed that the Commercial feed spacer always led to a thicker and denser biofilm on the membrane surface; followed by the Arch spacer case with less biofilm; whilst the Arch-Hole spacer had the thinnest biofilm. This indicated the Arch-Hole feed spacer resulted in least biofouling accumulation on the membrane, which was consistent with the macroscopic observations illustrated in Fig. 6.

The biofouling was further quantified and compared with TOC and ATP measurements for three cases. The ATP concentration associated with the biofouling differed with the different spacers. ATP concentration on membrane with the Commercial feed spacer was used as the baseline and was set to be one hundred percent. The values for the Arch and Arch-Hole cases were 71% and 21% respectively. It can be seen that Arch-Hole showed significant advantages in mitigating fouling on the membrane surface. The TOC concentration on the membrane surfaces with Arch-Hole spacers is 0.028 mg/cm^2 (26%) less than that with an Arch

feed spacer, and 0.073 mg/cm^2 (49%) less than that with a commercial design. Moreover, the TOC on the feed spacers themselves showed a similar trend for the different spacers. For any given spacer the value for the membrane surface was lower than that of the membrane surface indicating that biological fouling is somewhat more likely to occur on the membrane surface than the spacer which accords with [11]. That the fouling on the membrane itself is more serious accords with fouling being (at least in part) a flux driven process [47].

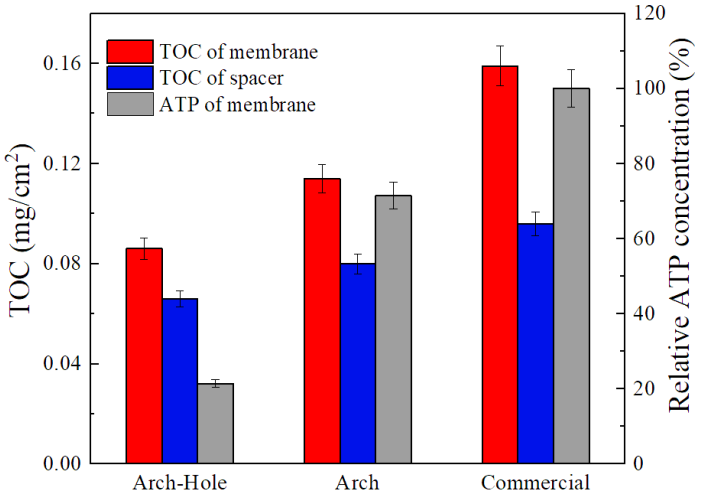

Fig.8 TOC concentration and ATP concentration of spacer and membrane after the membrane and spacer were fouled over a 5-day period. The TOC concentration on the spacer is based upon the underlying membrane area.

The fouling accumulation results of Figs. 6 ~ 8 could be partially explained by the different hydrodynamics induced by the different feed spacers shown in Figs. 4 and 5. Due to its more uniform velocity distribution, and hence the more uniform shear stress, the fouling attenuation in the Arch-Hole case is the most efficient. Of particular note, the areas in the fluid

flow direction before and after node are only lightly fouled. This is attributed to the design feature that induces a micro jet after each node. This feature distinguishes the Arch-Hole design from that of the Arch. With the Commercial design, the feed spacer occupies more of the cross-section and thus for the same nominal crossflow velocity some of the actual fluid velocities and shear stresses are higher than in the other two cases but there are more dead-zones. The outcome was found to be greater foulant accumulation.

3.3 Filtration performance

The feed channel pressure drop (FCP) increased in all three cases during the 120 hrs experiments. This was only by a factor of 1.2 times for Arch-Hole, by 1.6 times for Arch but was 4.7 times for the Commercial design. As shown in Fig. 9 the experiment with the Commercial design started with a value of over 7 mbar and finished with a value of around 35 mbar. The other two cases had relatively small values of FCP initially and at the end of the experiments as shown in Fig. 9.

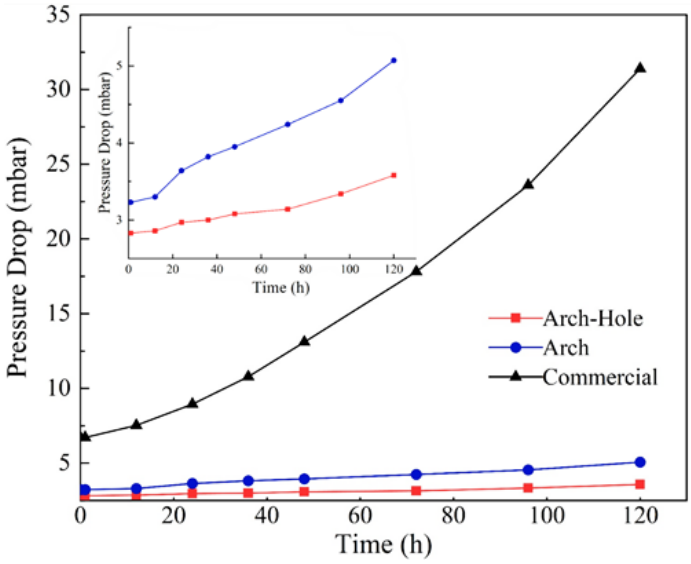

Fig. 9 Evolution of channel pressure drop over 5-days operation. Crossflow velocity: 0.12 m/s.

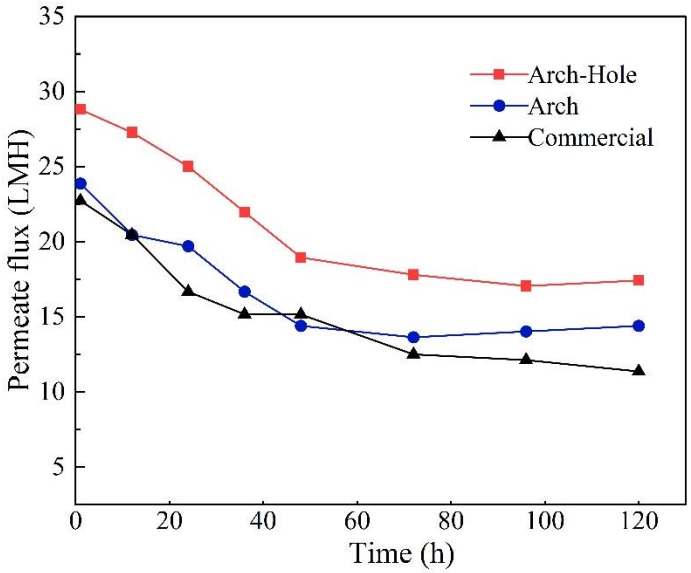

Fig. 10 Permeate flux as a function of time for three different spacers tested at a linear crossflow velocity of 0.12 m/s.

In Fig. 10, permeation flux was recorded during experiments, it can be seen that the flux first showed a downward trend and then stabilized. The sharp decrease in flux is because the pollutants in the feed water adsorb on the surface of the membrane and in the pores of the membrane, causing the total resistance to membrane fouling to increase. Owing to operation at constant pressure there is a consequential decrease in flux. That it reduced to a sustainable value corresponds with accepted theoretical expressions as explicated elsewhere [48] and accords with the concepts of critical and sustainable flux as discussed further in section 3.4.3. The modules with the Arch-Hole and Arch spacers tended to superior steady-state values. Given this finding, there is no conflict between choosing a design that minimizes capital cost, which corresponds to selecting the design or designs that maximize flux, and a design that minimizes operating cost which corresponds to selecting a design giving low channel pressure

drops.

The Specific Energy Consumption (SEC) for a product that is the permeate can be calculated from the following:

$$\mathrm{SEC} = \frac{Q_p \Delta P_{TM} + Q_f \Delta P_{FC}}{Q_p} \quad (5)$$

where Q_p and Q_f are the permeate and feed flowrates respectively, and ΔP_{TM} and ΔP_{FC} are the transmembrane and feed channel pressure drops respectively.

The system was operated with a transmembrane pressure drop of 0.76 MPa. Based upon the values at 120 hours and the above equation the SEC from Arch-Hole spacer is 0.26 kWh/m^3 which is significantly smaller than the 0.81 kWh/m^3 value with the commercial design of spacer. The Arch design has an intermediate value close to, but above that of Arch-Hole. It is 13% higher.

3.4 Discussion

3.4.1 Correlating spacer geometry and hydraulic performance

Filtration characteristics of pressure drop and specific flux have been compared in this work. Traditionally the optimal feed spacer design has been seen as a "trade-off" between mass transfer and channel pressure drop. However here it has been shown that achieving a high level of uniformity (coupled with the elimination of dead-zones) can lead to beneficial improvements in both flux and channel pressure drop.

To achieve this objective, the feed spacer was designed as an arch-type with streamlined

frame, which effectively optimized the attack/mesh angles and in particular made the velocity distribution more uniform. From Fig. 4, it can be seen that the Arch-Hole and Arch feed spacers have a more uniform velocity distribution compared to Commercial one, with dead zones essentially eliminated. Secondly, as a refinement, the Arch-Hole has an opening in the node. Unlike the hole design in a previous study [36, 37], the creation of the opening did not involve drilling through the node but was a passage created between two elliptical elements. The relatively wide opening avoided excessive changes in local velocities. The results from Figs. 4 ~ 10 confirmed this observation and demonstrated various favourable outcomes; having velocity distributions with only small fluctuations achieved beneficial results not only in channel pressure drop but also flux and SEC.

3.4.2 Shear stress and membrane fouling

Shear stress has an important influence on the development of fouling. Most scholars generally believe that high shear stress will reduce the initial adhesion of microorganisms and increase the chance of biofilms detaching from the surface. However, some scholars have emphasized that there is no “silver bullet” for biofouling [49]. Whilst the average shear stress was higher for the commercial design, Figs. 6 and 7 show that fouling with spacers of this design was more serious than that with the two novel designs. The implication is that the countervailing effects of dead-spaces is more important than the average value of shear stress. Furthermore, in the context of biofouling, a potentially important effect of shear stress is that it increases the boundary layer mass transfer coefficient (k) and reduces the nutrient concentration polarization (CP) next to the membrane [10]. Thus shear stress has not only an

effect on the initial adhesion of microorganisms but on their growth. Obviously, dead zones with low k and high CP will favour both initial attachment and then subsequent growth of the biofilm. It can be seen from Fig. 10 that the Arch-hole design with higher initial flux has the highest steady-state flux, and thus by implication improved mass transfer. It is recalled that Figs. 6 and 7 indicate that the foulant accumulation was less with the Arch-Hole design.

For very similar designs one would expect a link to average shear stress. and equally the elimination of potential dead-zones might be the key factor. As shown in Figs. 11 and 12, the differences in shear stress between Arch and Arch-Hole case are modest. As expected, Fig. 11 shows that Arch-Hole has a higher value at the node zone. Although the shear stress difference is not large, it is enough to have a noticeable effect on fouling (perhaps more specifically upon fouling initiation) and filtration performance.

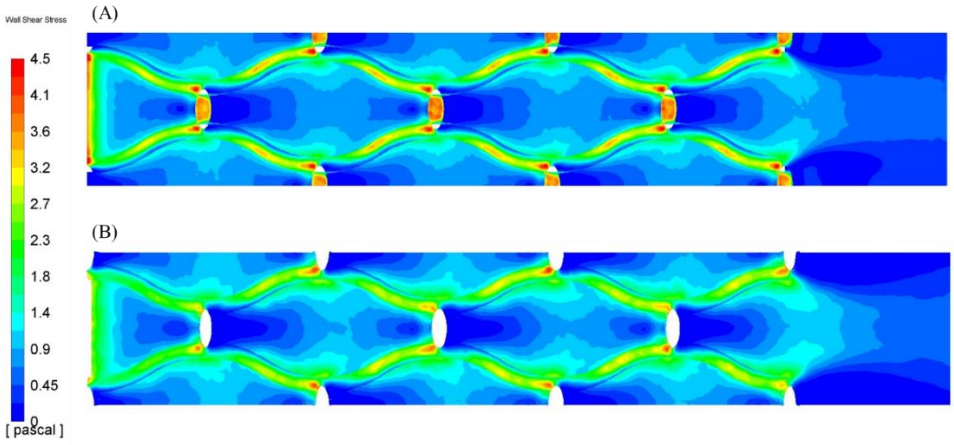

Fig.11 Comparison of shear stress contours at the membrane for a simulation at U_F = 0.12m/s: (A) Arch-Hole; (B) Arch.

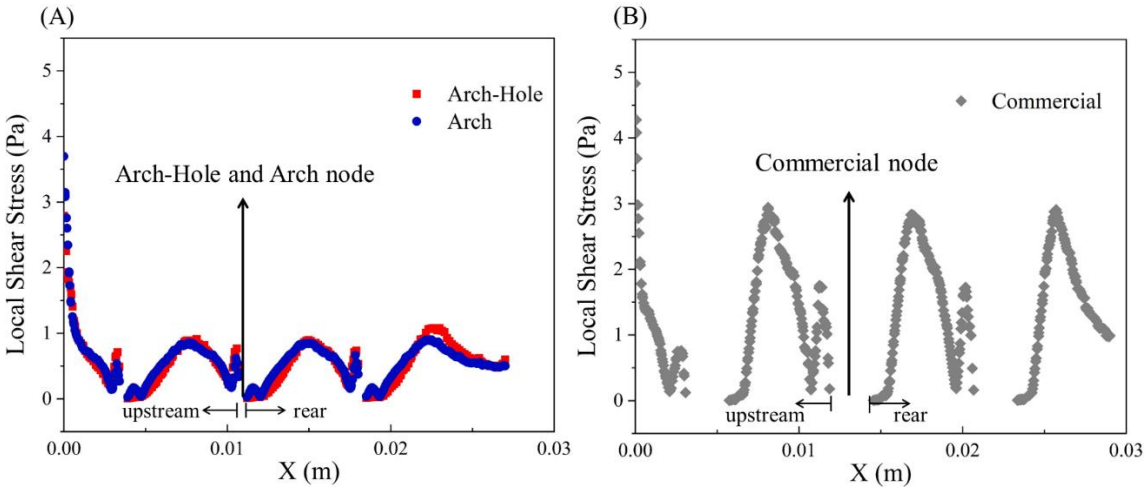

Fig.12 Shear stress simulation values for the center line of the membrane surface. (A) shows for Arch-Hole and Arch spacers the variation with position for the X direction. (B) shows the variation of shear stress in the X direction for the commercial design of spacer.

The variation of shear stress along the membrane is governed by the spacer design and shows peaks and troughs. As shown in Fig. 12 the variation for the new designs is distinct from the commercial design in at least two ways. The commercial design (Fig. 12 (B)) displays more intense peaks but also longer troughs whereas the new designs show a smoother near sinusoidal variation. The shear stress values upstream of the node are larger than those at the rear of the nodes indicating where liquid stagnation occurs and hence where bacterial growth will be promoted [50, 51].

3.4.3 Critical flux

In the process of studying membrane fouling, the concept of critical flux has been widely cited. The concept of critical flux was proposed by Field in 1995 [52], and its essence is that long-term operation of the membrane can best be achieved by selecting an appropriate

membrane flux that does not exceed the critical flux for that system. In further elaboration of, the concept of criticality, the threshold flux was proposed as an indication of the dividing point between low rates of fouling and high rates of fouling [53]. The critical flux is related to solute properties, hydraulic conditions and membrane properties. Whilst membrane fouling is often referred to as being 'flux-driven' (and it is the flux that does indeed 'drive' the process), the tendency towards a stable state is equally dependent upon the mass transfer conditions determining removal of foulants from the membrane surface as discussed in detail elsewhere e.g. appendix of [51].

In the present work the chosen operating pressure of 0.48 MPa gave initial fluxes between the two constant flux values of 20 and 35 LMH used in [11]. That the steady-state values in Fig. 10 for the new designs were found to be superior to that for the commercial design (and indeed the data for that design does not show a clear asymptote) is indicative of the enhanced mass transfer conditions generated by Arch-Hole and Arch spacers.

The tendency to a steady-state flux is not indicative of the strong form of the critical flux because consideration of the latter is only relevant for unfouled membranes. Tangential to this one may ask whether a fouling asymptote is indicative of an exhaustion of foulants. As the work reported here did involve the periodic addition of nutrients as mentioned in Section 2.2, the asymptotes are attributed to the new spacers creating an effective hydrodynamic environment rather than to any other factor. We also note that valid comparative conclusions can be drawn from the present data because the experimental set-up (Fig. 2) has a common feed tank for the three crossflow cells that are run in parallel. This certainly permits a comparison to be made between the three spacers. At full scale Arch-Hole and Arch may not

achieve the asymptotes demonstrated in Fig.10 but this can only be determined in full-scale long-term evaluations. However taken together Figs. 9 and 10 suggest that the new designs will have higher threshold fluxes for any given application. Firstly, because of lower foulant accumulation and secondly because as shown in Fig. 10, both Arch-Hole and Arch data displays genuine asymptotes whilst the data for the commercial design does not.

3.4.4 Mechanical Considerations

An important consideration is whether the mechanical stability of channels is still maintained with spacers having wide openings. There is a point at which greater spacer area will lead to collapse of channels. Also high pressures coupled with nodes of smaller area could lead to membrane punctures. As shown in Fig.12, all designs had the same density of nodes but the area of the nodes in the new design was smaller. In addition to the experiments reported here (which were run at 0.48 MPa) we have operated successfully at both 0.48 and 0.76 MPa with different NF membranes; there was no membrane perforation. The choice of 0.48 MPa for the present work was influenced by the fluxes that were generated (see previous section on critical flux) and not by any possible fragility of the new designs of spacers. The optimal applications for Arch-Hole and Arch designs will be determined by future work.

4. Concluding Remarks

Two new type feed spacers were developed in this work. They are Arch-Hole with a wide passage and a hole in the node, and Arch without such a passage (solid node). The analysis of the hydrodynamics, fouling and filtration performance leads to the following conclusions and

implications:

1) From CFD simulation results, more uniform velocity distribution and essentially no dead zones were obtained in Arch-Hole design. This resulted in less foulant accumulation as observed by OCT images (and as inferred from channel pressure drop measurements). The ATP and TOC measurements of Arch-Hole were 79% and 46% lower than those found for the commercial design, and 50% and 25% lower than for Arch.
2) The flow channel pressure drop increased with fouling in all cases but remained low for Arch-Hole and Arch designs. Arch-Hole value was lower by factors of 1.5 and 8.7 compared with the Arch and commercial case, respectively. Flux values associated with the various spacers were found to be as follows: Arch-Hole > Arch > commercial design.
3) Compared to the commercial one, use of the Arch-Hole design would reduce the energy cost of filtration by 69% for the application explored here. Also Arch has an SEC value 13% higher than Arch-Hole. For the foulant used, the results after 120 hours indicate that SEC with an Arch-Hole spacer is 0.26 kWh/m^3 compared with 0.81 kWh/m^3 for the commercial design of spacer. Furthermore for some applications displaying non-negligible osmotic pressure the saving in SEC could be greater The SEC values would be different because the *effective* osmotic pressure is affected by CP as well as the bulk solute concentration C_b, and the new designs generate better mass transfer conditions.
4) The current study explored the overall performance at constant pressure conditions. However, having demonstrated the potential benefits of the new designs, and in recognition of the fact that fouling can be very flux sensitive, further work at constant flux would be valuable.

Acknowledgements

This work was supported by grants from National Natural Science Foundation of China (No. 52100047); National Natural Science Foundation of China (No. 21706221). RWF acknowledges the support provided by an APEX project on water reuse that has been supported by the Royal Society in partnership with the British Academy and the Royal Academy of Engineering together with generous support from the Leverhulme Trust.

References

[1] Y.-H. Wang, Y.-H. Wu, X. Tong, T. Yu, L. Peng, Y. Bai, X.-H. Zhao, Z.-Y. Huo, N. Ikuno, H.-Y. Hu, Chlorine disinfection significantly aggravated the biofouling of reverse osmosis membrane used for municipal wastewater reclamation, Water Research, 154 (2019) 246-257.

[2] W. Lin, M. Li, Y. Wang, X. Wang, K. Xue, K. Xiao, X. Huang, Quantifying the dynamic evolution of organic, inorganic and biological synergistic fouling during nanofiltration using statistical approaches, Environment International, 133 (2019).

[3] W. Lin, Y. Zhang, D. Li, X.-m. Wang, X. Huang, Roles and performance enhancement of feed spacer in spiral wound membrane modules for water treatment: A 20-year review on research evolvement, Water Research, 198 (2021) 117146.

[4] Y. Gao, S. Haavisto, C.Y. Tang, J. Salmela, W. Li, Characterization of fluid dynamics in spacer-filled channels for membrane filtration using Doppler optical coherence tomography, Journal of Membrane Science, 448 (2013) 198-208.

[5] J.A.M. van Paassen, J.C. Kruithof, S.M. Bakker, F.S. Kegel, Integrated multi-objective membrane systems for surface water treatment: pre-treatment of nanofiltration by riverbank filtration and conventional ground water treatment, Desalination, 118 (1998) 239-248.

[6] J.S. Vrouwenvelder, D.A. Graf von der Schulenburg, J.C. Kruithof, M.L. Johns, M.C.M. van Loosdrecht, Biofouling of spiral-wound nanofiltration and reverse osmosis membranes: A feed spacer problem, Water Research, 43 (2009) 583-594.

[7] J.S. Vrouwenvelder, C. Hinrichs, W.G.J. Van der Meer, M.C.M. Van Loosdrecht, J.C. Kruithof, Pressure drop increase by biofilm accumulation in spiral wound RO and NF membrane systems: role of substrate concentration, flow velocity, substrate load and flow direction, Biofouling, 25 (2009) 543-555.

[8] J.S. Baker, L.Y. Dudley, Biofouling in membrane systems — A review, Desalination, 118 (1998) 81-89.

[9] X. Huang, G.R. Guillen, E.M.V. Hoek, A new high-pressure optical membrane module for direct observation of seawater RO membrane fouling and cleaning, Journal of Membrane Science, 364 (2010) 149-156.

[10] S.R. Suwarno, X. Chen, T.H. Chong, D. McDougald, Y. Cohen, S.A. Rice, A.G. Fane, Biofouling in reverse osmosis processes: The roles of flux, crossflow velocity and concentration polarization in biofilm development, Journal of Membrane Science, 467 (2014) 116-125.

[11] S.R. Suwarno, X. Chen, T.H. Chong, V.L. Puspitasari, D. McDougald, Y. Cohen, S.A. Rice, A.G. Fane, The impact of flux and spacers on biofilm development on reverse osmosis membranes, Journal of Membrane Science,

405-406 (2012) 219-232.
[12] A. Siddiqui, S. Lehmann, S.S. Bucs, M. Fresquet, L. Fel, E.I.E.C. Prest, J. Ogier, C. Schellenberg, M.C.M. van Loosdrecht, J.C. Kruithof, J.S. Vrouwenvelder, Predicting the impact of feed spacer modification on biofouling by hydraulic characterization and biofouling studies in membrane fouling simulators, Water Research, 110 (2017) 281-287.
[13] W.-c. Lin, R.-p. Shao, X.-m. Wang, X. Huang, Impacts of non-uniform filament feed spacers characteristics on the hydraulic and anti-fouling performances in the spacer-filled membrane channels: Experiment and numerical simulation, Water Research, 185 (2020).
[14] S. West, M. Wagner, C. Engelke, H. Horn, Optical coherence tomography for the in situ three-dimensional visualization and quantification of feed spacer channel fouling in reverse osmosis membrane modules, Journal of Membrane Science, 498 (2016) 345-352.
[15] G.A. Fimbres-Weihs, D.E. Wiley, Numerical study of mass transfer in three-dimensional spacer-filled narrow channels with steady flow, Journal of Membrane Science, 306 (2007) 228-243.
[16] P.R. Neal, H. Li, A.G. Fane, D.E. Wiley, The effect of filament orientation on critical flux and particle deposition in spacer-filled channels, Journal of Membrane Science, 214 (2003) 165-178.
[17] N. Horstmeyer, T. Lippert, D. Schoen, F. Schlederer, C. Picioreanu, K. Achterhold, F. Pfeiffer, J.E. Drewes, CT scanning of membrane feed spacers - Impact of spacer model accuracy on hydrodynamic and solute transport modeling in membrane feed channels, Journal of Membrane Science, 564 (2018) 133-145.
[18] K. Foo, Y.Y. Liang, G.A. Fimbres Weihs, CFD study of the effect of SWM feed spacer geometry on mass transfer enhancement driven by forced transient slip velocity, Journal of Membrane Science, 597 (2020).
[19] A. Subramani, S. Kim, E.M.V. Hoek, Pressure, flow, and concentration profiles in open and spacer-filled membrane channels, Journal of Membrane Science, 277 (2006) 7-17.
[20] P.A. Araujo, J.C. Kruithof, M.C.M. Van Loosdrecht, J.S. Vrouwenvelder, The potential of standard and modified feed spacers for biofouling control, Journal of Membrane Science, 403 (2012) 58-70.
[21] S. Kerdi, A. Qamar, A. Alpatova, J.S. Vrouwenvelder, N. Ghaffour, Membrane filtration performance enhancement and biofouling mitigation using symmetric spacers with helical filaments, Desalination, 484 (2020).
[22] Y.Y. Liang, G.A. Fimbres Weihs, D.E. Wiley, Comparison of oscillating flow and slip velocity mass transfer enhancement in spacer-filled membrane channels: CFD analysis and validation, Journal of Membrane Science, 593 (2020).
[23] M. Shakaib, S.M.F. Hasani, M. Mahmood, CFD modeling for flow and mass transfer in spacer-obstructed membrane feed channels, Journal of Membrane Science, 326 (2009) 270-284.
[24] C.P. Koutsou, S.G. Yiantsios, A.J. Karabelas, Numerical simulation of the flow in a plane-channel containing a periodic array of cylindrical turbulence promoters, Journal of Membrane Science, 231 (2003).
[25] B. Gu, C.S. Adjiman, X.Y. Xu, The effect of feed spacer geometry on membrane performance and concentration polarisation based on 3D CFD simulations, Journal of Membrane Science, 527 (2017) 78-91.
[26] A. Saeed, R. Vuthaluru, H.B. Vuthaluru, Investigations into the effects of mass transport and flow dynamics of spacer filled membrane modules using CFD, Chemical Engineering Research & Design, 93 (2015) 79-99.
[27] S.S. Bucs, R.V. Linares, J.O. Marston, A.I. Radu, J.S. Vrouwenvelder, C. Picioreanu, Experimental and numerical characterization of the water flow in spacer-filled channels of spiral-wound membranes, Water Research, 87 (2015) 299-310.
[28] C.P. Koutsou, S.G. Yiantsios, A.J. Karabelas, Numerical simulation of the flow in a plane-channel containing a periodic array of cylindrical turbulence promoters, Journal of Membrane Science, 231 (2004) 81-90.
[29] M. Shakaib, S.M.F. Hasani, M. Mahmood, Study on the effects of spacer geometry in membrane feed channels using three-dimensional computational flow modeling, Journal of Membrane Science, 297 (2007) 74-

89.
[30] Z. Cao, D.E. Wiley, A.G. Fane, CFD simulations of net-type turbulence promoters in a narrow channel, Journal of Membrane Science, 185 (2001) 157-176.
[31] M. Chai, Y. Ye, V. Chen, Separation and concentration of milk proteins with a submerged membrane vibrational system, Journal of Membrane Science, 524 (2017) 305-314.
[32] H.-Y. Tsai, A. Huang, J.F. Soesanto, Y.-L. Luo, T.-Y. Hsu, C.-H. Chen, K.-J. Hwang, C.-D. Ho, K.-L. Tung, 3D printing design of turbulence promoters in a cross-flow microfiltration system for fine particles removal, Journal of Membrane Science, 573 (2019) 647-656.
[33] Y.Z. Tan, Z. Mao, Y. Zhang, W.S. Tan, T.H. Chong, B. Wu, J.W. Chew, Enhancing fouling mitigation of submerged flat-sheet membranes by vibrating 3D-spacers, Separation and Purification Technology, 215 (2019) 70-80.
[34] S.M. Ali, A. Qamar, S. Kerdi, S. Phuntsho, J.S. Vrouwenvelder, N. Ghaffour, H.K. Shon, Energy efficient 3D printed column type feed spacer for membrane filtration, Water Research, 164 (2019).
[35] S.M. Ali, A. Qamar, S. Phuntsho, N. Ghaffour, J.S. Vrouwenvelder, H.K. Shon, Conceptual design of a dynamic turbospacer for efficient low pressure membrane filtration, Desalination, 496 (2020).
[36] S. Kerdi, A. Qamar, J.S. Vrouwenvelder, N. Ghaffour, Fouling resilient perforated feed spacers for membrane filtration, Water Research, 140 (2018) 211-219.
[37] A. Qamar, S. Kerdi, S.M. Ali, H.K. Shon, J.S. Vrouwenvelder, N. Ghaffour, Novel hole-pillar spacer design for improved hydrodynamics and biofouling mitigation in membrane filtration, Scientific Reports, 11 (2021).
[38] J.S. Vrouwenveder, J.A.M. van Paassen, J.M.C. van Agtmaal, M.C.M. van Loosdrecht, J.C. Kruithof, A critical flux to avoid biofouling of spiral wound nanofiltration and reverse osmosis membranes: Fact or fiction?, Journal of Membrane Science, 326 (2009) 36-44.
[39] I.S. Ngene, R.G.H. Lammertink, M. Wessling, W.G.J. Van der Meer, Particle deposition and biofilm formation on microstructured membranes, Journal of Membrane Science, 364 (2010) 43-51.
[40] N.M. Farhat, M. Staal, A. Siddiqui, S.M. Borisov, S.S. Bucs, J.S. Vrouwenvelder, Early non-destructive biofouling detection and spatial distribution: Application of oxygen sensing optodes, Water Research, 83 (2015) 10-20.
[41] C. Picioreanu, J.S. Vrouwenvelder, M.C.M.v. Loosdrecht, Three-dimensional modeling of biofouling and fluid dynamics in feed spacer channels of membrane devices, Journal of Membrane Science, 345 (2009).
[42] N. Thomas, N. Sreedhar, O. Al-Ketan, R. Rowshan, R.K. Abu Al-Rub, H. Arafat, 3D printed spacers based on TPMS architectures for scaling control in membrane distillation, Journal of Membrane Science, 581 (2019) 38-49.
[43] E.H.C. Castillo, N. Thomas, O. Al-Ketan, R. Rowshan, R.K. Abu Al-Rub, L.D. Nghiem, S. Vigneswaran, H.A. Arafat, G. Naidu, 3D printed spacers for organic fouling mitigation in membrane distillation, Journal of Membrane Science, 581 (2019) 331-343.
[44] W.S. Tan, S.R. Suwarno, J. An, C.K. Chua, A.G. Fane, T.H. Chong, Comparison of solid, liquid and powder forms of 3D printing techniques in membrane spacer fabrication, Journal of Membrane Science, 537 (2017) 283-296.
[45] R.V. Linares, S.S. Bucs, Z. Li, M. AbuGhdeeb, G. Amy, J.S. Vrouwenvelder, Impact of spacer thickness on biofouling in forward osmosis, Water Research, 57 (2014) 223-233.
[46] A. Magic-Knezev, D. van der Kooij, Optimisation and significance of ATP analysis for measuring active biomass in granular activated carbon filters used in water treatment, Water Research, 38 (2004) 3971-3979.
[47] F. Wicaksana, A.G. Fane, P. Pongpairoj, R. Field, Microfiltration of algae (Chlorella sorokiniana): Critical flux, fouling and transmission, Journal of Membrane Science, 387-388 (2012) 83-92.

[48] J.J. Wu, Improving membrane filtration performance through time series analysis, Discover Chemical Engineering, 1 (2021) 7.
[49] H.C. Flemming, M. Meier, T. Schild, Mini-review: microbial problems in paper production, Biofouling, 29 (2013) 683-696.
[50] T. Saur, E. Morin, F. Habouzit, N. Bernet, R. Escudié, Impact of wall shear stress on initial bacterial adhesion in rotating annular reactor, PloS one, 12 (2017) e0172113.
[51] A.I. Radu, J.S. Vrouwenvelder, M. van Loosdrecht, C. Picioreanu, Modeling the effect of biofilm formation on reverse osmosis performance: Flux, feed channel pressure drop and solute passage, Journal of Membrane Science, 365 (2010) 1-15.
[52] R.W. Field, D. Wu, J.A. Howell, B.B. Gupta, Critical flux concept for microfiltration fouling, Journal of Membrane Science, 100 (1995) 259-272.
[53] R.W. Field, G.K. Pearce, Critical, sustainable and threshold fluxes for membrane filtration with water industry applications, Advances in colloid and interface science, 164 (2011) 38-44.